PHYSICAL REVIEW C **89**, 014313 (2014)

Coulomb excitation of neutron-rich Cd isotopes

S. Ilieva,[1,*] M. Thürauf,[1] Th. Kröll,[1,2] R. Krücken,[2] T. Behrens,[2] V. Bildstein,[2,3] A. Blazhev,[4] S. Bönig,[1] P. A. Butler,[5] J. Cederkäll,[6] T. Davinson,[7] P. Delahaye,[6] J. Diriken,[8,9] A. Ekström,[10] F. Finke,[4] L. M. Fraile,[11] S. Franchoo,[12] Ch. Fransen,[4] G. Georgiev,[13] R. Gernhäuser,[2] D. Habs,[14] H. Hess,[4] A. M. Hurst,[5,15] M. Huyse,[8] O. Ivanov,[8] J. Iwanicki,[16] P. Kent,[17] O. Kester,[14] U. Köster,[6] R. Lutter,[14] M. Mahgoub,[2] D. Martin,[4] P. Mayet,[8] P. Maierbeck,[2] T. Morgan,[14] O. Niedermeier,[3] M. Pantea,[1] P. Reiter,[4] T. R. Rodríguez,[1] Th. Rolke,[4] H. Scheit,[3] A. Scherillo,[4,18] D. Schwalm,[3] M. Seidlitz,[4] T. Sieber,[6] G. S. Simpson,[18] I. Stefanescu,[8] S. Thiel,[4] P. G. Thirolf,[14] J. Van de Walle,[8] P. Van Duppen,[8] D. Voulot,[6] N. Warr,[4] W. Weinzierl,[2] D. Weisshaar,[4] F. Wenander,[6] A. Wiens,[4] and S. Winkler[2]

[1]*Institut für Kernphysik, Technische Universität Darmstadt, Germany*
[2]*Physik-Department E12, Technische Universität München, Garching, Germany*
[3]*Max-Planck-Institut für Kernphysik, Heidelberg, Germany*
[4]*Institut für Kernphysik, Universität zu Köln, Germany*
[5]*Oliver Lodge Laboratory, University of Liverpool, United Kingdom*
[6]*CERN, Genève, Switzerland*
[7]*Department of Physics and Astronomy, University of Edinburgh, United Kingdom*
[8]*Instituut voor Kern- en Stralingsfysica, KU Leuven, Belgium*
[9]*Belgian Nuclear Research Centre SCK·CEN, Mol, Belgium*
[10]*Fysiska Institutionen, Lunds Universitet, Sweden*
[11]*Grupo de Física Nuclear, Universidad Complutense de Madrid, Madrid, Spain*
[12]*Institut de Physique Nucléaire d'Orsay, Orsay, France*
[13]*CSNSM, CNRS/IN2P3, Université Paris-Sud, UMR8609, F-91405 ORSAY-Campus, France*
[14]*Ludwig-Maximilians-Universität München, Garching, Germany*
[15]*Lawrence Berkeley National Laboratory, Berkeley, California, USA*
[16]*Środowiskowe Laboratorium Ciężkich Jonów, Uniwersytet Warszawski, Poland*
[17]*Nuclear Physics Group, Department of Physics, University of York, United Kingdom*
[18]*Laboratoire de Physique Subatomique et de Cosmologie, Grenoble, France*

(Received 20 December 2013; published 21 January 2014)

The isotopes ^{122,124,126}Cd were studied in a "safe" Coulomb-excitation experiment at the radioactive ion-beam facility REX-ISOLDE at CERN. The reduced transition probabilities $B(E2;0^+_{\mathrm{g.s.}} \rightarrow 2^+_1)$ and limits for the quadrupole moments of the first 2^+ excited states in the three isotopes were determined. The onset of collectivity in the vicinity of the $Z = 50$ and $N = 82$ shell closures is discussed by comparison with shell model and beyond mean-field calculations.

DOI: 10.1103/PhysRevC.89.014313　　PACS number(s): 25.70.De, 27.60.+j, 23.20.−g, 21.10.Ky

I. INTRODUCTION

The region of the nuclear chart around the doubly magic nucleus ^{132}Sn is of special interest for nuclear physics. Due to the proximity to the closed shells $Z = 50$ and $N = 82$, it is expected that the structure of these nuclei can be described as few-particles/holes configurations coupled to the ^{132}Sn core. When approaching the $N = 82$ shell closure following the cadmium isotopic chain ($Z = 48$), an anomalous behavior of the energies of the first excited state 2^+_1 is observed, with the energy in ^{128}Cd being lower than the one in ^{126}Cd. On the other side of $Z = 50$, the Te isotopes ($Z = 52$), which have two valence protons, show the "normal" behavior of increasing excitation energies when approaching a shell closure. The comparison between the energies of the 2^+ states and model predictions for Cd may indicate a possible quenching of the spherical $N = 82$ shell closure when moving away from the valley of stability [1]. Besides the nuclear structure interest, the understanding of the nuclei around the doubly magic isotope ^{132}Sn is also important for the understanding of nucleosynthesis processes. The mass calculations from [2], which also include shell quenching, led to a considerable improvement of the solar element abundances in r-process calculations [3]. The spherical shell quenching in the r-process waiting point nuclei needs to be confirmed experimentally.

When the $N = 82$ cadmium isotope ^{130}Cd became experimentally accessible, based on the agreement between the measured Q_β value with a couple of theoretical calculations, Dillmann *et al.* [4] concluded that this is an evidence of shell quenching. The subsequent measurements of the masses of the cadmium isotopes at ISOLTRAP, CERN, disagree with this hypothesis and show no irregularities but a smooth decrease in the mass excess towards the $N = 82$ shell closure [5]. Recent measurements of the excitation scheme of ^{130}Cd following the decay of the 8^+ isomer also showed no evidence of a reduction of the $N = 82$ shell gap [6] and shell-model calculations are able to reproduce these experimental results very well. Jungclaus *et al.* [6] propose that the anomaly in the 2^+ energy in ^{128}Cd is caused by the presence of quadrupole

---

*silieva@ikp.tu-darmstadt.de

collectivity close to the $N = 82$ shell closure rather than by shell quenching. Beyond mean-field calculations are also able to explain the $E(2^+)$ anomaly in the Cd isotopes without using quenching of the $N = 82$ shell closure [7]. However, they predict that the cadmium isotopes are weakly deformed. This is quite surprising considering the proximity of these isotopes to the $Z = 50$ and $N = 82$ shell closures. For a long time the cadmium isotopes were considered as a textbook example for spherical vibrational nuclei based on the existing information on their excited states [8]. A more detailed recent analysis, including more data on transition rates and branching ratios in the midshell region, put some doubt on this simple picture concerning multiphonon states [9].

To study the evolution of nuclear structure and possible deformation around the $Z = 50$ and $N = 82$ shell closures, not only the energies of the 2_1^+ excited states but also the evolution of the $B(E2; 0^+_{\text{g.s.}} \rightarrow 2_1^+)$ values is of paramount importance. As it is a challenge to produce the neutron-rich cadmium isotopes towards $N = 82$, the heaviest isotope with a known $B(E2)$ value prior to the present experiment was ^{122}Cd. In this work we proceeded further towards the $N = 82$ shell closure. The development of RIB facilities, such as REX-ISOLDE at CERN, allows for Coulomb excitation studies of many new isotopes. In fact, such measurements in heavy-mass nuclei have become standard within the last decade [10,11]. Low-energy Coulomb-excitation measurements of even-even isotopes are sensitive to the $\langle 2_1^+ || \mathcal{M}(\mathrm{E2}) || 0^+_{\text{g.s.}} \rangle$, and to a certain extent to the $\langle 2_1^+ || \mathcal{M}(\mathrm{E2}) || 2_1^+ \rangle$ matrix elements. Hence, also information on the shape of the nucleus can be deduced. In two experimental campaigns, the reduced transition probabilities in the isotopes ^{124}Cd and ^{126}Cd were measured for the first time and the already known $B(E2)$ value in ^{122}Cd [12] was remeasured as a reference.

II. EXPERIMENTAL METHOD

A. Radioactive ion-beam production and experimental setup for Coulomb-excitation measurements

The two experiments were performed at the ISOL radioactive ion-beam facility REX-ISOLDE at CERN. For the production of the cadmium isotopes a heated UC$_x$/graphite target ($\approx$50 g/cm^2 ^{238}U and $\approx$10 g/cm^2 carbon) was used. A 1.4 GeV proton beam, provided by the PS-Booster, hit a tungsten rod, used as a neutron converter to enhance the Cd yield, and a cocktail of isotopes was produced following neutron-induced fission of the target. The average intensity of the proton beam was 3×10^{13} protons/pulse. The isotopes produced diffuse out of the target at different rates depending on their chemical properties. For the Cd case, the use of a neutron converter reduces the amount of isobaric cesium contamination in the beam. During the second experimental campaign, a new quartz transfer line was used at the primary target, which significantly improved the beam quality reducing the cesium content of the beam to a negligible amount. The suppression of Cs was proven in a separate measurement with a ΔE-E telescope, consisting of an ionization chamber and a silicon surface barrier detector [11,13]. However, in this measurement the Cd and In isotopes could not be separated, therefore no quantitative estimation of the beam composition was possible. To determine the beam composition other methods were used (see Sec. II B). The selective ionization of the cadmium atoms using RILIS (Resonant Ionization Laser Ion Source) enhances the cadmium content extracted from the primary target [14]. After ionization, the singly charged ions are extracted with 30 kV, mass separated in the general purpose separator (GPS) and then sent to the REX postaccelerator [15].

At REX-ISOLDE the ions are first cooled and bunched in a Penning trap (REXTRAP) and then charge bred in the Electron Beam Ion Source (EBIS) to a mass-to-charge ratio smaller than $\approx$4.5, which is the limit of the REX-LINAC. For the cadmium beams charge states 30^+ (^{124}Cd) and 31^+ (^{122}Cd and ^{126}Cd) were used. A breeding time of 250 ms was necessary to reach these charge states. For the most exotic isotope studied in the present experiment, ^{126}Cd, which has a half-life of $T_{1/2} = 0.515$ s, this leads to about 28% in-trap decay of the cadmium inside the EBIS. This decay together with the isobars coming from the primary target contribute to the contamination in the beam. After a second mass separation, the beam is postaccelerated in the REX-LINAC up to an energy of 2.85 MeV/nucleon and then sent to the Miniball setup for the Coulomb-excitation experiment.

At the Miniball setup [11] (Fig. 1), the emitted γ rays are detected in a germanium detector array (Miniball) and the ejectiles and recoils are detected in a double-sided silicon-strip detector (DSSSD) [16]. Miniball consists of eight cluster detectors, each of them containing three individually encapsulated HPGe crystals. The clusters are arranged in a close geometry (covering $\approx$60% of the total solid angle) around a target chamber that contains a target wheel and the particle detector. The total efficiency of the Ge detector array is around 7% at 1.3 MeV. The DSSSD consists of four individual detectors (quadrants) with a thickness of 500 μm. Each quadrant is segmented on the front side in 16 annular rings and on the back side in 24 radial strips. Each pair of strips is coupled together and in total 12 radial read-out signals are available. This corresponds to an azimuthal angular resolution in ϕ of 6.8°. The rings have a pitch of 2 mm and the innermost ring has an inner radius of 9 mm. The average distance between the secondary target and the particle detector was 31 mm which corresponds to an angular coverage $15^\circ < \theta_{\text{lab}} < 50^\circ$.

The first excited states in ^{122,124,126}Cd were populated via "safe" Coulomb excitation. The beams of ^{122}Cd and ^{124}Cd bombarded 2 mg/cm^2 ^{108}Pd and ^{104}Pd targets, respectively. These targets were chosen because of the optimal Coulomb-excitation cross section they provide at the energy achievable with REX-ISOLDE. In the second measurement, a 1.8 mg/cm^2 ^{64}Zn target was used for the study of ^{124}Cd and ^{126}Cd. Even though this target does not provide the highest Coulomb-excitation cross section, it was chosen as it allows a kinematic separation of particle and target nuclei in the detector setup, which was not the case with the palladium targets. In a semi-classical treatment the condition for safe Coulomb excitation can be interpreted geometrically such that the nuclei should always be kept at a distance $b(\theta) \geqslant R_1 + R_2 + \Delta$ from each other, with a safety distance $\Delta \approx 5$ fm for heavy systems [17]. The semi-classical treatment of our projectile-target systems can be justified as the Sommerfeld parameter is $\eta \sim 130$ for

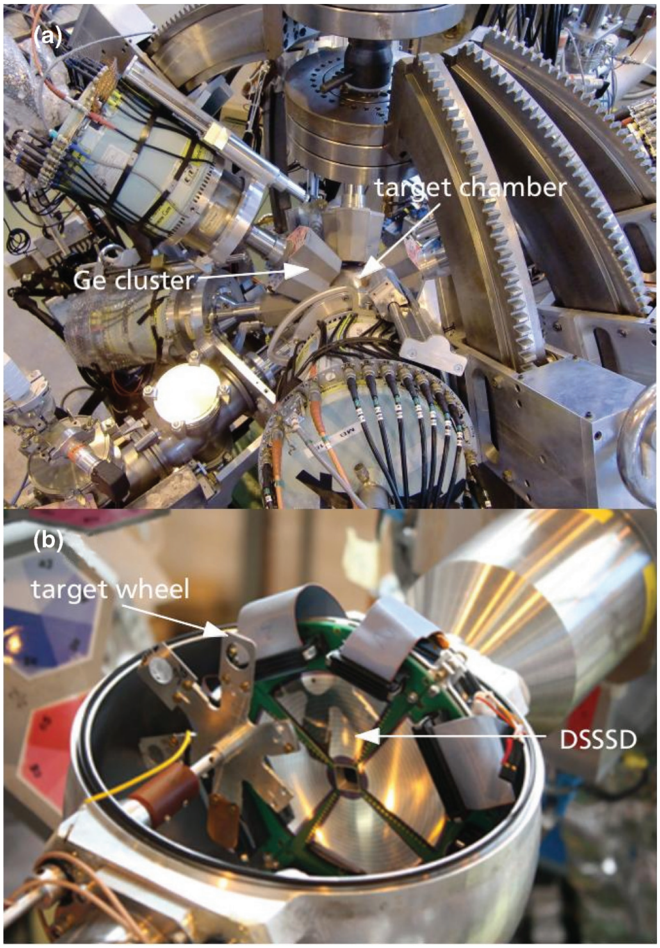

FIG. 1. (Color online) Miniball setup. (a) Target chamber for the Coulomb excitation setup, surrounded by the Ge cluster detectors. (b) Particle detector (DSSSD) and target wheel inside the target chamber.

the Zn target and $\eta \sim 200$ for the Pd target (for "safe" Coulex it is necessary that $\eta \gg 1$). With our experimental conditions and for the observable center-of-mass angles $\Delta \geqslant 15$ fm was always fulfilled and a contribution from nuclear interaction could be excluded.

B. Data analysis

The beam delivered to the Miniball setup was not isotopically pure. Several methods can be used to determine the amount of isobaric contamination in the beam. The first one uses the fact that when the RILIS laser is off, due to its higher ionization potential compared to cesium and indium, almost no cadmium is extracted from the target. Therefore, only the isobaric contaminants, which are easily surface ionized, are present in the beam. In Fig. 2 the prompt γ-ray spectrum detected in coincidence with particles in the DSSSD for the $A = 122$ beam is shown as an example, measured in laser-on [(blue) solid line] and laser-off [(red) dashed line] mode. The transition from the deexcitation of the first 2^+ state in ^{122}Cd at 569 keV, which is clearly visible in the "laser on" spectrum, disappears when the laser is off. By comparing the intensity of the target excitation (γ-ray line at 434 keV) or the number of elastically scattered projectiles in the DSSSD with laser on and off, the amount of isobaric contamination in the beam can be determined. For the ^{126}Cd beam, one also has to take into account the decay of this isotope in the EBIS and correct the beam composition accordingly.

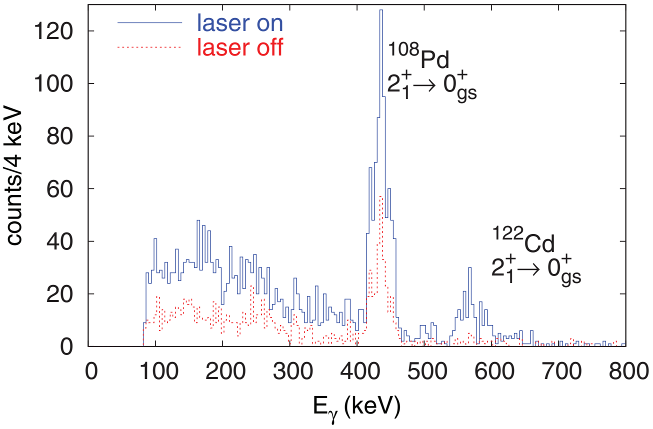

FIG. 2. (Color online) Prompt γ-ray spectrum in coincidence with particles from the ^{122}Cd measurement (no Doppler correction is applied). The (blue) solid line shows the spectrum taken in laser-on mode and the (red) dashed one in laser-off mode.

Another method to determine the beam composition uses the fact that the isotopes in the provided beam are unstable and undergo a β decay. This method has higher systematic uncertainty compared to the previous one, as the γ rays are not emitted from a point-like source, rather from particles scattered throughout the target chamber. Therefore, the efficiency calibration obtained with a point-like ^{152}Eu source cannot be used for the decay study. However, with a simultaneous fit of the efficiency and the amount of each isotope to the γ-ray yields following the β decay, the relative amount of each isotope in the beam can be determined. The method could only be used for the ^{124,126}Cd beams because ^{122}Cd decays directly to the ground state of ^{122}In and no γ rays are observed in this case. The mean values for the fraction of cadmium ions in the beam for each mass are given in Table I.

During the experiment it was found that the beam was not positioned exactly in the center of the target. For the determination of the scattering angles of the particles, needed later for Doppler correction and differential cross section

TABLE I. Properties of the beams used. The beam intensity N_{Cd} represents the amount of cadmium isotopes reaching the secondary target at Miniball. The fraction of cadmium isotopes in the beam is f_{Cd}. The relatively low yield N_{Cd} of ^{124}Cd on the ^{64}Zn target is due to the aging of the production target towards the end of the experiment.

Beam	Target	E_{tot} (MeV)	N_{Cd} (pps)	f_{Cd} (%)	Isobaric contaminants
^{122}Cd	^{108}Pd	347.7	1.0×10^4	58(1)	In, Cs
^{124}Cd	^{104}Pd	353.4	2.4×10^3	18(1)	In, Cs
^{124}Cd	^{64}Zn	353.4	6.6×10^3	79(4)	In
^{126}Cd	^{64}Zn	359.1	1.1×10^4	45(1)	In

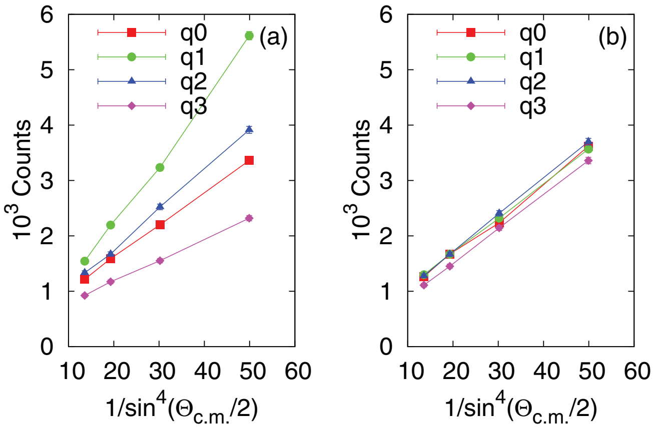

FIG. 3. (Color online) Total number of events in the Rutherford scattering peak in the particle detector as a function of $1/\sin^4(\Theta_{\mathrm{c.m.}}/2)$. Without an offset the angular ranges correspond to strips numbers 3, 4, 5, and 6 for each quadrant of the DSSSD detector. The lines are to guide the eye. The shape follows the Rutherford scattering cross section. (a) With the beam assumed to be passing through the geometric center of the DSSSD, (b) with the corrected beam position.

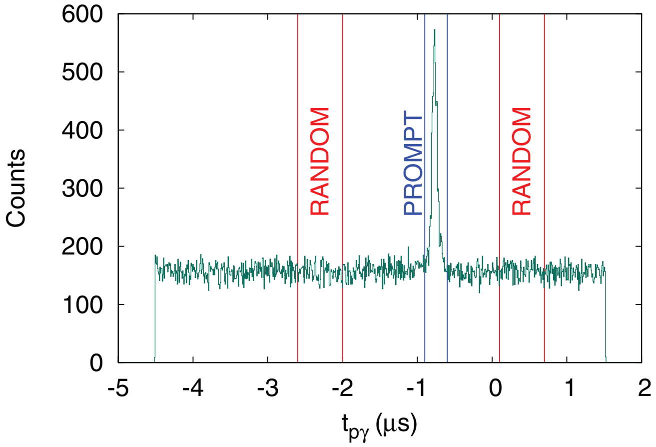

FIG. 4. (Color online) Particle-γ time-difference spectrum. The windows of prompt and random coincidences are indicated.

$(d\sigma/d\Omega)$ determination, the exact beam position is necessary. To determine the beam shift, the number of elastically scattered particles in several intervals $\Delta\theta_{\mathrm{lab}}$, corresponding to the width of one ring in the DSSSD, were compared for the four quadrants. For each quadrant the numbers should follow the Rutherford (elastic) cross section and, when the beam is in the center, the number of events for each interval in the different quadrants should be the same. In Fig. 3(a) the correlation assuming that the beam passes through the geometric center of the target is plotted. Different rates are observed in the four quadrants, which shows that the beam was off center. The same correlation, after correcting the beam position, is shown in Fig. 3(b). In this case the same rates are observed in all quadrants, as expected. Beam shifts of the order of 1.5 mm were observed for the different beams.

The finite size of the beam spot also has an effect on the correct scattering angle determination. With a Monte Carlo simulation it was estimated that the contribution of this effect is smaller than the uncertainty arising from the strip size. Hence, in the following analysis, a point-like beam was assumed.

Data with absolute time stamps from a 40-MHz clock were collected during the beam time [11]. The data were sorted offline in particle-γ coincident events within a 6-μs time window. The particle-γ time-difference spectrum is shown in Fig. 4. Prompt coincidences were selected using a 220-ns gate in the particle-γ time spectrum. The γ-ray detection efficiency was increased by using an offline add-back scheme. Due to the pulse-height deficit [18] and the dead layer of the silicon detectors, it is very difficult to make a proper energy calibration for heavy ions. The energy of the particles, used for Doppler correction, was calculated from the angles measured with the DSSSD using the correlations for inelastic scattering kinematics. The type of the detected particle (ejectile or recoil) was determined from the deposited energy versus scattering-angle correlation (Fig. 5). However, this was possible only in the measurements with ^{124,126}Cd beams on the zinc target. For the palladium targets no kinematic separation was possible. As a result, it was not possible to make a good Doppler correction, which, especially for the ^{124}Cd case where the energies of the $2_1^+ \rightarrow 0_1^+$ transitions in the projectile and the target lie very close, hindered the estimation of the γ-ray yields for the transitions.

The final results of the analysis are the prompt γ-ray spectra with subtracted random background (normalized to the width of the prompt window) shown in Fig. 6. The energies of the γ rays are Doppler corrected with respect to the velocity of the emitting nucleus, reconstructed from the measured scattering angle. The results of the measurement of the Coulomb excitation reaction of ^{122}Cd on ^{108}Pd target are shown in Fig. 6(a). The spectrum is free from radioactive decay background and only the $2_1^+ \rightarrow 0_{\mathrm{g.s.}}^+$ transitions in the projectile and the target are present. The tail on the cadmium peak is a result of the incomplete Doppler correction, due to the insufficient kinematic separation of the projectile and target nuclei. In Fig. 6(b), the result from the measurement of ^{124}Cd on a ^{64}Zn target is plotted. Again, only the transitions from the first excited state to the ground state in the projectile and

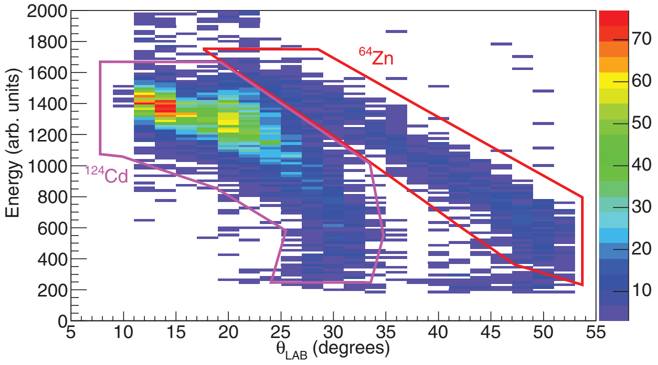

FIG. 5. (Color online) Particle energy vs. scattering angle for the $A = 124$ beam on a ^{64}Zn target. The scattered projectiles can be clearly separated from the recoiling target nuclei.

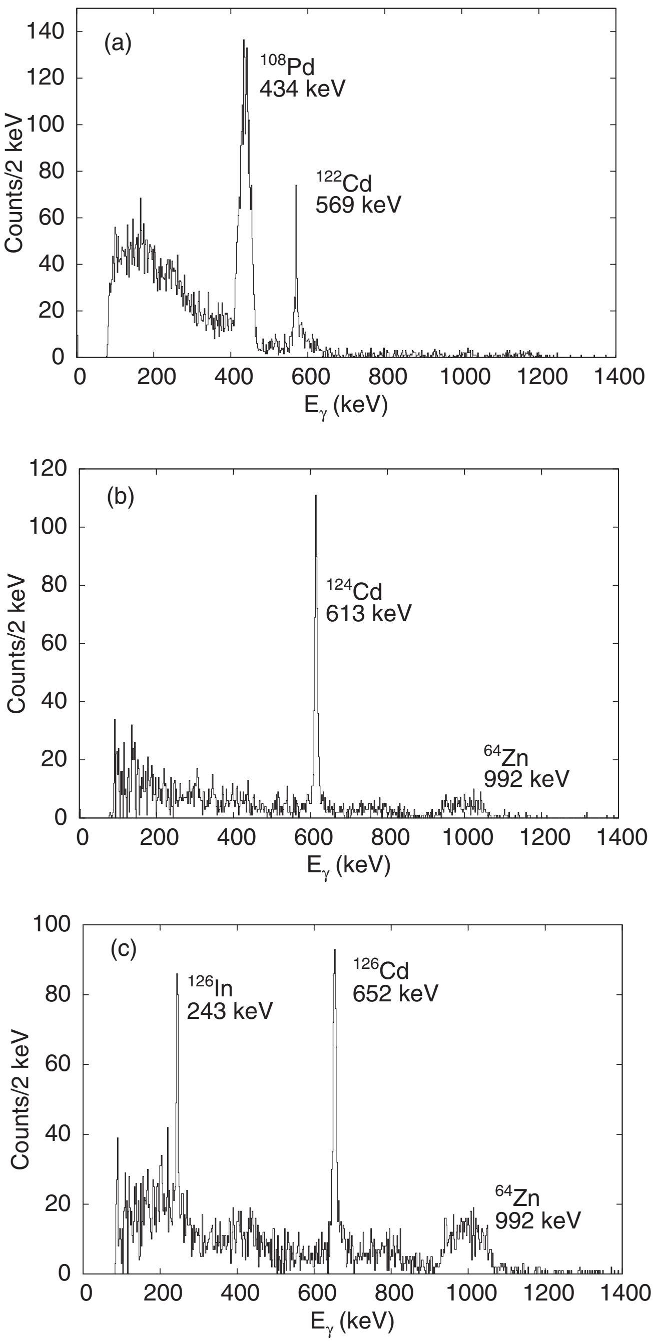

FIG. 6. Background-subtracted projectile Doppler-corrected γ-ray spectra taken in laser-on mode for the (a) ^{122}Cd, (b) ^{124}Cd, and (c) ^{126}Cd measurement, respectively. The energies of the $2_1^+ \to 0_{\rm g.s.}^+$ transitions in the projectile and target nuclei are indicated.

TABLE II. Experimental relative γ-ray yields as extracted from the data.

Measurement	γ-ray yield		$\theta_{\rm lab}$ (°)
	projectile $2_1^+ \to 0_{\rm g.s.}^+$	target $2_1^+ \to 0_{\rm g.s.}^+$	
^{122}Cd + ^{108}Pd	781(28)	1780(45)	15–52
^{124}Cd + ^{104}Pd	82(9)	138(6)	15–32
	46(7)	98(5)	33–51
^{124}Cd + ^{64}Zn	63(8)	27(5)	18–24
	93(10)	35(6)	27–50
^{126}Cd + ^{64}Zn	235(15)	131(11)	10–24
	396(20)	251(16)	20–50

target nuclei are present. For the $A = 126$ beam (see Fig. 6(c)), besides the γ rays associated with the $2_1^+ \to 0_{\rm g.s.}^+$ transition in ^{64}Zn and ^{126}Cd, there is an additional transition at 243 keV assigned to the Coulomb excitation of the ^{126}In isotope, which was present in the beam as well. This transition was previously reported by Hellström *et al.* [19] and Scherillo *et al.* [20] and was tentatively assigned to the decay of a 30 μs isomer in the indium isotope. In both cases the isomeric state has been populated from above. In the present experiment the transition appears to be prompt (it can be observed when the spectrum is Doppler-corrected with respect to the projectile velocity) and it is populated via Coulomb excitation. This implies that there is another transition (possibly with low energy) between the isomer and the 243 keV state which was not seen in the previous measurements. Details on the observation of the In isotope will be published elsewhere. The yields for the transitions in projectiles and targets from the different measurements are summarized in Table II. The conversion coefficients at the excitation energies in the cadmium isotopes are much smaller than 0.005 and conversion electron correction has no impact on our results [21].

III. ANALYSIS AND RESULTS

A. Coulomb-excitation cross section

As a measure for the Coulomb-excitation cross section, the integrated particle-γ coincidences, detected in the Miniball setup, are used. The cross section for Coulomb excitation of the projectile, σ_P, is determined relative to the cross section for the target excitation, σ_T, that is already known, according to the relation

$$\sigma_P = \sigma_T \frac{N_\gamma^P}{\varepsilon_\gamma^P} \frac{\varepsilon_\gamma^T}{N_\gamma^T} \frac{1}{f_{\rm Cd}}, \tag{1}$$

where $N_\gamma^{P,T}$ are the experimental γ-ray yields for the $2_1^+ \to 0_{\rm g.s.}^+$ transitions in the projectile and the target. In Eq. (1), $f_{\rm Cd}$ represents the fraction of cadmium ions in the beam and $\varepsilon_\gamma^{P,T}$ are the relative efficiencies of the Ge detectors at the energies of the $2_1^+ \to 0_{\rm g.s.}^+$ transitions in the projectile and target nuclei, respectively. This method has the advantage that no absolute γ-ray detection efficiency or dead-time correction are needed. The Miniball cluster detectors are placed at angles where the effect of the deorientation of the nuclear states is the smallest, therefore, the total yield is not affected by the change in the angular distribution of the γ rays.

To calculate the Coulomb-excitation cross sections, the CLX/DCY code [22], which is based on the original Winther and de Boer code [23], was used. The calculations take into account the energy loss in the target. The cross section is a function of a transition matrix element M_{20} and a diagonal matrix element M_{22}, which are connected to the reduced transition probability $B(E2)$ and the spectroscopic quadrupole moment of the 2_1^+ state Q_s via the relations

$$M_{20} = \langle 2_1^+ \| \mathcal{M}(E2) \| 0_{\text{g.s.}}^+ \rangle = \sqrt{B(E2; 0_{\text{g.s.}}^+ \to 2_1^+)}$$

$$M_{22} = \langle 2_1^+ \| \mathcal{M}(E2) \| 2_1^+ \rangle = \sqrt{\frac{7}{2\pi}} \frac{5}{4} e Q_s(2_1^+) \, .$$

The Coulomb-excitation cross section for the target is calculated using the already known matrix elements (see Sec. III B). Then, using Eq. (1), the experimental cross section for the projectile excitation is determined. Afterwards, a map of possible pairs of the transition M_{20} and diagonal M_{22} matrix elements is determined with a fit to the experimental cross section.

Other matrix elements were not included in the calculation. At the final beam energy of 2.85 MeV/nucleon, which is much smaller than the energy for "safe" Coulomb excitation, deexcitation from higher-lying excited states was not observed in the data. The effect of this feeding was studied by comparing the results of the CLX/DCY calculations with and without higher-lying states included. The contribution to the M_{22} and M_{20} matrix elements is an order of magnitude smaller than the uncertainty of our measurement. Therefore, feeding of the 2_1^+ excited state from above was not taken into account in the subsequent analysis.

B. Determination of the transition and diagonal matrix elements

The matrix elements M_{20} and M_{22}, used to calculate the Coulomb-excitation cross section for the employed targets, are listed in Table III. The quadrupole moment of the 2_1^+ state in ^{108}Pd has been studied in a number of experimental works [24–28]. Two values for the quadrupole moments were given, one obtained with constructive interference between the direct excitation of the first 2^+ state and excitation via the second 2^+ state and the other one with destructive interference. The authors of references [24–26] find that there is more evidence supporting constructive interference, therefore, for the current analysis the value for the diagonal matrix element is calculated as a weighted mean of the quadrupole moments from all the above mentioned studies obtained with constructive interference. The values from destructive interference were not taken into account.

TABLE III. Target parameters used for the calculations of the Coulomb-excitation cross section.

Target	d (mg/cm^2)	M_{20} (eb)	M_{22} (eb)
^{104}Pd	2.0	0.731(24)[a]	−0.33(12)[b]
^{108}Pd	2.0	0.872(11)[a]	−0.666(33)[c]
^{64}Zn	1.8	0.406(4)[a]	−0.013(100)[d]

[a] $B(E2)$ value from Ref. [29].

[b] From Ref. [30].

[c] Weighted mean value from [24–28].

[d] From the results in Ref. [31].

For the ^{64}Zn target, two measurements of the quadrupole moment of the 2_1^+ excited state via Coulomb excitation with inconsistent results exist. The measurement of Salém-Vasconcelos *et al.* [32] resulted in a rather large quadrupole moment [mean value $Q_s(2_1^+) = -0.29(4)$ eb], while Koizumi *et al.* [31] give a value consistent with zero. We studied the excitation probability by comparing the number of elastically scattered particles (Rutherford cross section) with the number of deexcitation γ rays from the target (Coulomb excitation cross section) from our measurement. This procedure results in better agreement of the experimental ratio of the measured cross sections with the calculated ratio when the quadrupole moment of the ^{64}Zn is assumed to be zero. For this calculation it was assumed that the excitation probability for ^{64}Zn does not change with the charge of the projectile in our case ($Z = 48$ and $Z = 49$). Even though our experiment was not optimized to extract a precise value of the quadrupole moment $Q_s(2^+)$ from the absolute cross section, based on the above considerations we used a vanishing quadrupole moment for the 2^+state in ^{64}Zn, as given in [31], to obtain the results presented in this paper. The same analysis with the large quadrupole moment of the 2_1^+ state in ^{64}Zn decreases the deduced quadrupole moment for the 2_1^+ state in the cadmium isotopes by about an order of magnitude while the determined $B(E2)$ values for the excitation of this state remain the same within error bars.

Taking into account the proximity of the cadmium isotopes studied to the closed shells $Z = 50$ and $N = 82$, we first analyzed the data for each isotope assuming that the quadrupole moment of the 2_1^+ state is zero. The transition matrix element M_{20} was varied until the experimental values for the measured deexcitation rate were reproduced. The results for the three cadmium isotopes are given in Table IV. The errors include statistical errors and systematic uncertainties, that are due to the error in the determined beam composition and the efficiencies of the Ge detectors.

A more independent approach to determine the transition M_{20} and diagonal M_{22} matrix elements is the maximum likelihood method [33]. The likelihood function $\mathcal{L}$ is defined as

$$\mathcal{L}(M_{20}, M_{22}) = \prod_{i=1}^{N} f(x_i; M_{20}, M_{22}), \tag{2}$$

TABLE IV. Transition and diagonal matrix elements for the $0_{\text{g.s.}}^+ \to 2_1^+$ transition in the cadmium isotopes.

Isotope	M_{20} (eb), if $M_{22} = 0$ (eb)	Estimators	
		M_{20} (eb)	M_{22} (eb)
^{122}Cd	0.636(20)	$0.64^{+0.16}_{-0.17}$	$-0.04^{+4.0}_{-2.0}$
^{124}Cd	0.594(38)	$0.59^{+0.15}_{-0.18}$	$0.09^{+3.9}_{-2.0}$
^{126}Cd[a]	0.536(17)	$0.53^{+0.07}_{-0.08}$	$0.10^{+1.7}_{-1.1}$
^{126}Cd[b]	0.535(17)	$0.52^{+0.05}_{-0.07}$	$0.35^{+1.4}_{-0.9}$

[a] Without lifetime constraint.

[b] With lifetime constraint.

where $f(x_i; M_{20}, M_{22})$ is the probability density function (p.d.f.) of the unknown parameters M_{20} and M_{22} for i independent data sets x_i. For the p.d.f a Gaussian distribution with a standard deviation determined from the statistical error of the γ-ray yields and the systematic errors coming from efficiency calibration and the uncertainty in the beam composition was assumed. The effect of the matrix elements on the Coulomb-excitation cross section is quite different at small and large center-of-mass angles. Therefore, the measurements of the cross section at small and large center-of-mass angles were used as independent data sets. In the cases where the lifetime of the first 2_1^+ state is known, a third independent distribution was constructed with this data. The maximum likelihood estimators are found by solving the equation

$$\frac{\partial \ln \mathcal{L}}{\partial M_{20,22}} = 0 . \tag{3}$$

The 1σ contour for the likelihood function is described by the solution of the equation

$$\ln \mathcal{L} = \ln \mathcal{L}_{\max} - 1/2 . \tag{4}$$

We applied the maximum likelihood method to the data, but due to the low statistics quite large 1σ contours are obtained, what leads to large uncertainties in the determined matrix elements, in particular the diagonal ones. The description of this analysis for each isotope follows and at the end the estimators for M_{20} and M_{22} are given.

a. ^{122}Cd The Coulomb-excitation cross section for the excitation of the 2_1^+ state in the ^{122}Cd isotope was calculated varying the transition matrix element M_{20} from 0 *e*b up to 1.2 *e*b, and the diagonal matrix element M_{22} from -4 *e*b to 4 *e*b. Sets of matrix elements (M_{20}, M_{22}), that reproduce the experimental cross section, were determined throughout these ranges. The experimental cross section was measured in the range $31^\circ < \Theta_{\text{c.m.}} < 150^\circ$ (the range limits vary $\pm 4^\circ$ for the different quadrants of the particle detector as the beam was not passing through the geometric center of the detector) and it was used to construct the first probability function for the maximum likelihood analysis. A second function for the likelihood analysis was constructed assuming a constant M_{20} matrix element, corresponding to the measured lifetime of 15±7 ps [12] ($M_{20} = 0.670 \pm 0.156$ *e*b), for the entire range of M_{22} values. The resulting 1σ contour is plotted in Fig. 7(a) and the values for the estimators are presented in Table IV. The maximum-likelihood ellipse does not close on the positive side of M_{22} values, but as values outside of the plotted range are unphysical this region was not studied and is not shown in the figure.

b. ^{124}Cd In the case of ^{124}Cd, the measurements with different targets provided the possibility for the construction of several independent probability density functions. With the ^{64}Zn target, the Coulomb-excitation cross section was determined for small ($54.9^\circ < \Theta_{\text{c.m.}} < 76.1^\circ$) and large ($79.6^\circ < \Theta_{\text{c.m.}} < 125.5^\circ$) scattering angles. Ranges that do not overlap are chosen, so that the effect of the quadrupole moment of the 2^+ excited state on the Coulomb-excitation cross section is enhanced. The same was done for the data on the ^{104}Pd target where one function for the ranges $33^\circ < \Theta_{\text{c.m.}} < 71^\circ$ and $115.6^\circ < \Theta_{\text{c.m.}} < 148^\circ$, which due to the kinematics could not be separated, was constructed. The second function was for the range $73.5^\circ < \Theta_{\text{c.m.}} < 113.7^\circ$. The results are presented

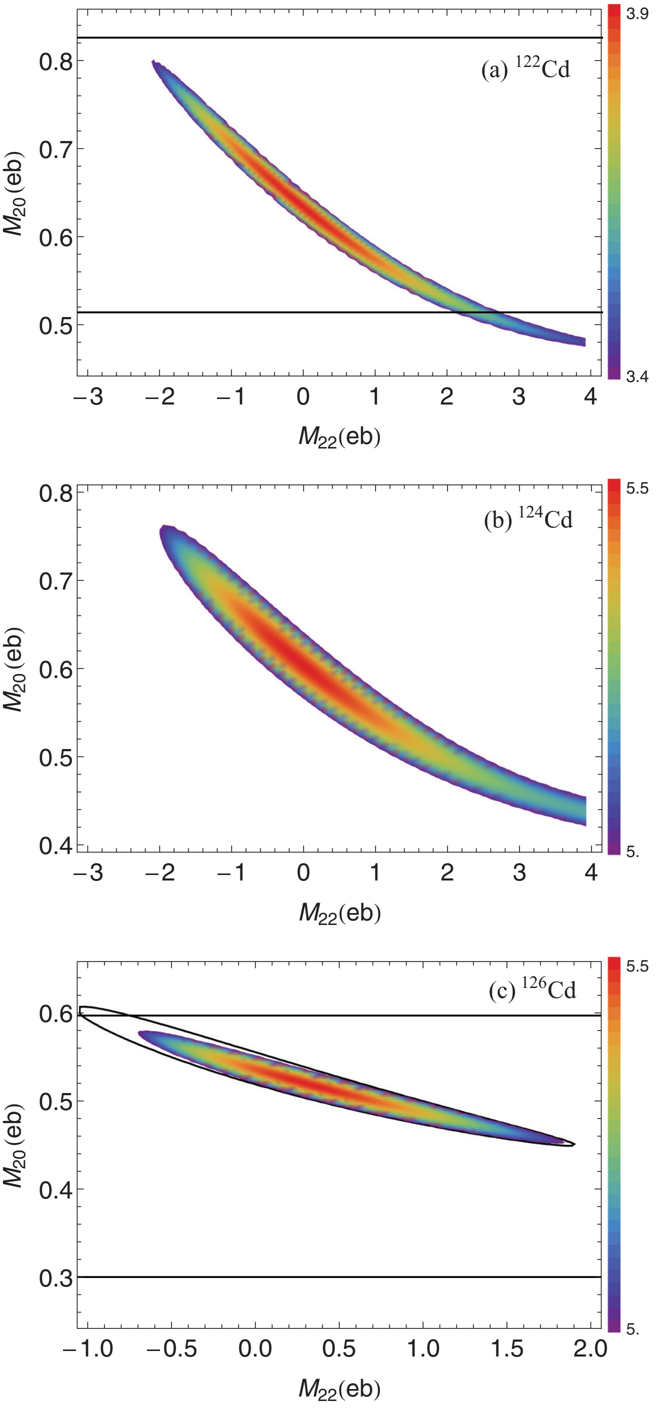

FIG. 7. (Color online) 1σ regions determined with the maximum-likelihood approach, for the diagonal M_{22} and transition M_{20} matrix elements for the 2_1^+ state in (a) ^{122}Cd, (b) ^{124}Cd, and (c) ^{126}Cd. The error ellipses determine the possible combinations of M_{22} and M_{20} values for each isotope. For ^{126}Cd two ellipses are shown—solid line contour, which includes only the Coulomb excitation data in the likelihood function and a density plot, created with a likelihood function which contains also the lifetime p.d.f. The solid lines in (a) and (c) represent the 1σ boundary for M_{20} derived from lifetime measurements.

in Fig. 7(b) and in Table IV. It should be noted that also in this case the ellipse does not close at high M_{22} values, due to the small statistics of the measurement.

c. ^{126}Cd Two of the maximum likelihood functions for ^{126}Cd were built from the data measured at small ($38^\circ < \Theta_{\text{c.m.}} < 77^\circ$) and large ($79.5^\circ < \Theta_{\text{c.m.}} < 139.5^\circ$) scattering angles. For the third one, the $B(E2)$ value calculated from the lifetime of the 2_1^+ state was used.

The lifetime of the 2_1^+ state was determined in a recent Coulomb-excitation experiment at Miniball with a ^{126}Cd beam on a thick ^{64}Zn target using the Doppler-shift attenuation method (DSAM) [34]. The predictions for the lifetime of the 2_1^+ state are 9.6 ps (using the Raman rule [29]) or 13 ps (see Sec. IV, Grodzins rule). Hence, this method was chosen for a first attempt to measure the lifetime directly. For the measurement only 20 of the Miniball Ge detectors were working. In a standard DSAM setup all detectors are placed at the same θ angle and the spectra can be summed which gives the advantage of having higher statistics. That is an essential difference to the Miniball setup where all the detectors have different angles. Thus, the spectra from the different detectors cannot be added which results in much lower statistics for the individual angles. However, with the newly developed DSAM-code APCAD [35] the data from a multi-angle measurement can be analyzed by simultaneously fitting all the spectra.

The fit of the peak shape was performed using the HYPERMET function [36], which consists of a Gaussian function with an additive tail, as it describes best the detector response. The lineshape depends on the angle of the emitted photon with respect to the trajectory of the projectile, the kinetic energy of the projectile and the lifetime of the excited state. The angular distribution of the γ rays was taken into account. The trajectory and the stopping process can be calculated in a Monte Carlo simulation based on GEANT4, which gives the stopping matrix. Using this matrix and the θ and ϕ angles of the detectors, one can calculate the lineshape of a transition with the lifetime as a free parameter. The only other free parameter is the sum intensity of the transition in all the 20 detectors. As the intensities of the peaks in the different detectors are not fitted separately and due to the low statistics, the fits at different angles have different quality and do not always reproduce the measured intensity. The analysis resulted in a lifetime

$$\tau(2_1^+) = \left(14.9\left({}^{+16.8}_{-5.0}\right)_{\text{stat}} \pm 0.7_{\text{model}}\right)\ \text{ps}$$

and the corresponding χ^2 distribution is shown in Fig. 8. The statistical error is determined by a change in the χ^2 values with one unit. The model error is due to the uncertainty in the stopping power. The DSAM method is best applicable for shorter lifetimes of the order of 10 ps or less. Due to the obviously too long lifetime of ^{126}Cd and the low statistics of the measurement, the result has a large error. One can see that only a lower limit of the lifetime of 9.2 ps can be given with confidence. The upper limit of the lifetime cannot be determined reliably. Small uncertainties in the calculated stopping power and the high statistical error lead to big changes in the upper limit of the lifetime resulting in a flat χ^2 distribution. From this new experimental finding, we can conclude that for a more precise lifetime measurement the recoil-distance Doppler-shift method is much better suited.

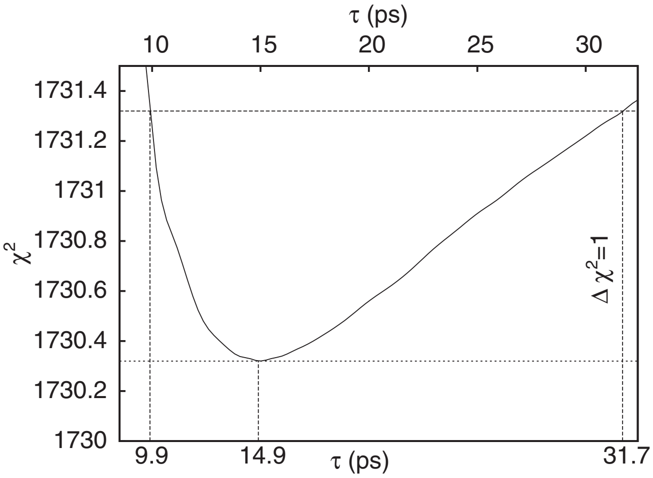

FIG. 8. χ^2 distribution for the DSAM fits ($\chi^2_{\text{red,min}} = 1.23$). At $\tau = 9.9$ ps and $\tau = 31.7$ ps the value of χ^2 has changed by 1, which determines the standard deviation of the lifetime of the 2^+ state ($\tau_{2^+} = 14.9$ ps).

Figure 7(c) shows the 1σ contour for the matrix elements for ^{126}Cd and the estimators are listed in Table IV. A much smaller $B(E2)$ value as compared to the other two cadmium isotopes is obtained. Small quadrupole moments consistent with zero were determined for all three isotopes (Table IV) and no considerable deformation could be observed.

IV. THEORETICAL INTERPRETATION AND DISCUSSION

The information on the $B(E2; 0^+_{\text{g.s.}} \rightarrow 2^+_1)$ values in the neutron-rich Cd isotopes towards the closed shell $N = 82$ is summarized in Fig. 9 and in Table V. We determined a transition strength of 22.7(83) W.u. in ^{122}Cd, which is consistent

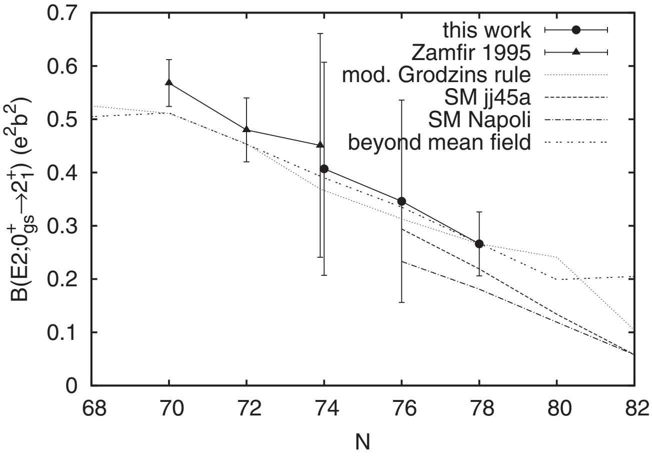

FIG. 9. Systematics of the $B(E2; 0^+_{\text{g.s.}} \rightarrow 2^+_1)$ values for the cadmium isotopic chain as a function of the neutron number. The results from the shell-model calculation are marked with SM followed by the name of the interaction used in the calculation; Zamfir 1995 shows the results from Ref. [12].

TABLE V. Comparison of the experimental transition probabilities $B(E2;0^+_{\text{g.s.}} \rightarrow 2^+_1)$ and the spectroscopic quadrupole moments $Q_s(2^+_1)$ of the 2^+_1 excited state in the cadmium isotopes with shell model and beyond mean-field [7] calculations.

Isotope	Experimental values		Theoretical predictions			
			Shell model *jj45pna*		Beyond mean field	
	$B(E2)$ (e^2b^2)	Q_s (eb)	$B(E2)$ (e^2b^2)	Q_s (eb)	$B(E2)$ (e^2b^2)	Q_s (eb)
^{122}Cd	0.41(20)	$-0.03^{+3.0}_{-1.6}$	–	–	0.390	−0.446
^{124}Cd	0.35(19)	$0.07^{+2.9}_{-1.5}$	0.294	0.228	0.335	−0.418
^{126}Cd[a]	0.27(6)	$0.27^{+1.1}_{-0.7}$	0.219	0.094	0.267	−0.415

[a] With lifetime constraint.

with the previous measurement, and in ^{124}Cd and ^{126}Cd, which were measured for the first time, strengths of 18.8(75) W.u. and 14.3(24) W.u., respectively. The experimental results from this work are compared with the systematics values obtained using a modified Grodzins rule [37] and with several theoretical calculations.

The Grodzins systematics allows for an estimation of the collectivity of a state. It relates small transition energies to large transition probabilities and vice versa. The modified Grodzins rule gives the $B(E2;0^+_{\text{g.s.}} \rightarrow 2^+_1)$ value as

$$B(E2;0^+_{\text{g.s.}} \rightarrow 2^+_1)[e^2\text{b}^2] = 2.57\frac{Z^2}{A^{2/3}}\frac{1}{E_{2^+_1}[\text{keV}]}\,(1.288 - 0.088(N - \tilde{N}))\,,$$

where $\tilde{N}$ is the neutron number for which the mass within an isobaric chain reaches its minimum and the numerical coefficients are determined from a fit to the experimentally known $B(E2;0^+_{\text{g.s.}} \rightarrow 2^+_1)$ values in this mass region [37]. The expected decrease in the transition strength towards the shell closure is observed. Our results are relatively close to the systematics and follow the same trend.

The transition strengths $B(E2)$ and the quadrupole moments $Q_s(2^+_1)$ in the neutron-rich cadmium isotopes were calculated using the shell model and a beyond mean-field approach. Within the shell model, two interactions were used, namely the $jj45pna$ [38] and *Napoli* interactions [20,39–41]. For the effective charges $e_\pi = 1.35$ and $e_\nu = 0.78$ were used, as in Ref. [41]. The results with the two interactions are identical at the shell closure and the difference increases when going away from it (Fig. 9).

The beyond mean-field (BMF) calculation was performed using a symmetry conserving configuration mixing approach [7]. Particle number and angular momentum restoration, as well as axial quadrupole shape mixing were taken into account. The interaction (Gogny D1S [42]) was adjusted to reproduce global properties (masses and radii) of some selected nuclei but can be applied along the whole nuclear chart without additional fine tunings.

The experimental $B(E2)$ values are well reproduced by the BMF calculations and even by the simple Grodzins systematics (see Fig. 9). Shell-model calculations, which are available only starting from ^{124}Cd, are a bit lower than the measured transition strength. In both ^{124}Cd and ^{126}Cd, a collectivity higher than the one predicted by the shell model observed, which is surprising for nuclei that are a small number of valence holes away from the closed shells $Z = 50$ and $N = 82$.

Although successful in the prediction of transition strengths, the BMF calculations overestimate the quadrupole deformation in the studied Cd isotopes. They predict a large prolate deformation of the first excited states in the cadmium isotopes in the vicinity of the shell closure but experimentally rather spherical shape is observed. This is in agreement with the results from a laser spectroscopy measurement of ground-state quadrupole moments in the odd-mass Cd isotopes [43]. High-precision lifetime measurements for the three isotopes would help determine the value of the quadrupole moment of the first excited state with much smaller uncertainty, when available.

V. SUMMARY

In an experiment at REX-ISOLDE, CERN, the reduced transition probabilities $B(E2;0^+_{\text{g.s.}} \rightarrow 2^+_1)$ for the excitation of the 2^+_1 state in the isotopes ^{122,124,126}Cd were measured using Coulomb excitation. The obtained values are 0.41(20) e^2b^2, 0.35(19) e^2b^2, and 0.27(6) e^2b^2, for ^{122}Cd, ^{124}Cd, and ^{126}Cd, respectively. Furthermore, a first attempt to measure the quadrupole moments of the first 2^+ states was made. The quadrupole moments, although determined with high uncertainties, are in agreement with the quadrupole moments observed in the odd-mass cadmium isotopes. Comparison with several theoretical approaches shows that a beyond mean-field theory describes experimental observations to a high degree of agreement. The evolution of the $B(E2)$ values with increasing neutron number has the expected behavior of decreasing transition strengths and shows no indication for possible shell quenching at $N = 82$. Even though moderate collectivity is observed, which is unusual for nuclei with so few valence holes away from the closed shells, the measured quadrupole moments indicate a spherical rather than deformed shape, as opposed to the BMF theoretical predictions. To completely discard the possibility for a reduction of the $N = 82$ shell gap, the transition probabilities in the last two cadmium isotopes up to the shell closure, ^{128}Cd and ^{130}Cd, need to be determined.

ACKNOWLEDGMENTS

This work was partly supported by the German Federal Ministry of Education and Research (BMBF) with Grant Nos. 06DA9036I, 05P12RDCIA, 06MT190, 06MT238, 05P09PKCI5, and 05P12PKFNE, the European Union under EURONS (No. 506065) and ENSAR (No. 262010), Spanish MINECO FPA2010-17142 and the UK Science and Technology Facilities Council.

---

[1] T. Kautzsch *et al.*, Eur. Phys. J. A **9**, 201 (2000).

[2] J. Dobaczewski, I. Hamamoto, W. Nazarewicz, and J. A. Sheikh, Phys. Rev. Lett. **72**, 981 (1994).

[3] B. Chen, J. Dobaczewski, K.-L. Kratz, K. Langanke, B. Pfeiffer, F.-K. Thielemann, and P. Vogel, Phys. Lett. B **355**, 37 (1995).

[4] I. Dillmann, K.-L. Kratz, A. Wöhr, O. Arndt, B. A. Brown, P. Hoff, M. Hjorth-Jensen, U. Köster, A. N. Ostrowski, B. Pfeiffer, D. Seweryniak, J. Shergur, W. B. Walters, and the ISOLDE Collaboration, Phys. Rev. Lett. **91**, 162503 (2003).

[5] M. Breitenfeldt *et al.*, Phys. Rev. C **81**, 034313 (2010).

[6] A. Jungclaus *et al.*, Phys. Rev. Lett. **99**, 132501 (2007).

[7] T. R. Rodríguez, J. L. Egido, and A. Jungclaus, Phys. Lett. B **668**, 410 (2008).

[8] A. Aprahamian, D. S. Brenner, R. F. Casten, R. L. Gill, and A. Piotrowski, Phys. Rev. Lett. **59**, 535 (1987).

[9] P. E. Garrett and J. L. Wood, J. Phys. G: Nucl. Part. Phys. **37**, 064028 (2010).

[10] P. van Duppen and K. Riisager, J. Phys. G: Nucl. Part. Phys. **38**, 024005 (2011).

[11] N. Warr *et al.*, Eur. Phys. J. A **49**, 40 (2013).

[12] N. V. Zamfir, R. L. Gill, D. S. Brenner, R. F. Casten, and A. Wolf, Phys. Rev. C **51**, 98 (1995).

[13] W. Weinzierl, Diploma Thesis, TU Munich, 2006.

[14] U. Köster *et al.*, Nucl. Instrum. Methods Phys. Res. B **204**, 347 (2003).

[15] D. Habs *et al.*, Nucl. Instrum. Methods Phys. Res. B **139**, 128 (1998).

[16] A. N. Ostrowski, S. Cherubini, T. Davinson, D. Groombridge, A. M. Laird, A. Musumarra, A. Ninane, A. di Pietro, A. C. Shotter, and P. J. Woods, Nucl. Instrum. Methods Phys. Res. A **480**, 448 (2002).

[17] W. Wilcke, J. Birkelund, H. Wollersheim, A. Hoover, J. Huizenga, W. Schröder, and L. Tubbs, At. Data Nucl. Data Tables **25**, 389 (1980).

[18] G. Pasquali, G. Casini, M. Bini, S. Calamai, A. Olmi, G. Poggi, A. Stefanini, F. Saint-Laurent, and J. Steckmeyer, Nucl. Instrum. Methods Phys. Res. A **405**, 39 (1998).

[19] M. Hellström, M. Mineva, A. Blazhev, H. Boardman, J. Ekman, K. Gladnishki, H. Grawe, J. Gerl, R. Page, Z. Podolyak, and D. Rudolph, *Proceedings of the Third International Conference on Fission and Properties of Neutron-rich Nuclei* (World Scientific, Singapore, 2002), p. 22.

[20] A. Scherillo, J. Genevey, J. A. Pinston, A. Covello, H. Faust, A. Gargano, R. Orlandi, G. S. Simpson, I. Tsekhanovich, and N. Warr, Phys. Rev. C **70**, 054318 (2004).

[21] T. Kibédi, T. W. Burrows, M. B. Trzhakovskaya, P. M. Davidson, and C. W. Nestor, Jr., Nucl. Instrum. Methods Phys. Res. A **589**, 202 (2008).

[22] H. Ower, CLX/DCY code (unpublished).

[23] A. Winther and J. de Boer, in *Coulomb Excitation*, edited by K. Alder and A. Winther (Academic Press, New York/London, 1966) Chap. A Computer Program for Multiple Coulomb Excitation, p. 303.

[24] W. R. Lutz, J. A. Thomson, R. P. Scharenberg, and R. D. Larsen, Phys. Rev. C **6**, 1385 (1972).

[25] R. P. Harper, A. Christy, I. Hall, I. M. Naqib, and B. Wakefield, Nucl. Phys. A **162**, 161 (1971).

[26] L. Hasselgren, C. Fahlander, F. Falk, L. O. Edvardson, J. E. Thun, B. S. Ghuman, and B. Skaali, Nucl. Phys. A **264**, 341 (1976).

[27] M. Maynard, D. C. Palmer, J. R. Cresswell, P. D. Forsyth, I. Hall, and D. G. E. Martin, J. Phys. G: Nucl. Phys. **3**, 1735 (1977).

[28] D. Ward, J. S. Geiger, and R. L. Graham, Bull. Amer. Phys. Soc. **16**, 14 (1971).

[29] S. Raman, C. W. Nestor, and P. Tikkanen, At. Data Nucl. Data Tables **78**, 1 (2001).

[30] A. Christy, I. Hall, P. R. Harper, I. M. Naqib, and B. Wakefield, Nucl. Phys. A **142**, 591 (1970).

[31] M. Koizumi *et al.*, JAERI Review **028**, 22 (2003).

[32] S. Salém-Vasconcelos, M. J. Bechara, J. H. Hirata, and O. Dietzsch, Phys. Rev. C **38**, 2439 (1988).

[33] J. Beringer *et al.* (Particle Data Group), Phys. Rev. D **86**, 010001 (2012).

[34] M. Thürauf, M.S. thesis, Technische Universität Darmstadt, 2012.

[35] C. Stahl, M.S. thesis, Technische Universität Darmstadt, 2011.

[36] R. Helmer and M. Lee, Nucl. Instrum. Methods **178**, 499 (1980).

[37] Th. Kröll *et al.*, Coulomb excitation of neutron-rich $A \approx 140$ nuclei. proposal to the INTC committee CERN-INTC-2004-026/P-156, 2004.

[38] M. Hjorth-Jensen, Shell Model Interaction (unpublished).

[39] A. Covello and A. Gargano (private communication).

[40] L. Coraggio, A. Covello, A. Gargano, N. Itaco, and T. T. S. Kuo, Phys. Rev. C **66**, 064311 (2002).

[41] J. Genevey, J. A. Pinston, H. R. Faust, R. Orlandi, A. Scherillo, G. S. Simpson, I. S. Tsekhanovich, A. Covello, A. Gargano, and W. Urban, Phys. Rev. C **67**, 054312 (2003).

[42] J. Berger, M. Girod, and D. Gogny, Nucl. Phys. A **428**, 23 (1984).

[43] D. T. Yordanov *et al.*, Phys. Rev. Lett. **110**, 192501 (2013).